

Two forsterite-bearing FUN inclusions in the Allende meteorite

ROBERT N. CLAYTON^{1,2,3}, GLENN J. MACPHERSON², IAN D. HUTCHEON^{3,5}, ANDREW M. DAVIS^{2,4},
LAWRENCE GROSSMAN^{2,3}, TOSHIKO K. MAYEDA³, CAROL MOLINI-VELSKO¹, JOHN M. ALLEN²

¹Department of Chemistry, ²Department of the Geophysical Sciences, ³Enrico Fermi Institute,

⁴James Franck Institute, University of Chicago, Chicago, IL 60637

and

AHMED EL GORESY

Max-Planck-Institut für Kernphysik, P.O.B. 103980, 6900 Heidelberg, Germany

(Received August 4, 1983; accepted in revised form December 9, 1983)

Abstract—We have discovered two FUN inclusions, CG-14 and TE, among a group of five forsterite-rich inclusions in Allende, two of which are described for the first time herein. All five consist of euhedral forsterite and spinel crystals poikilolithically enclosed by fassaite. Forsterite and spinel are usually segregated from one another, sometimes into a spinel-rich mantle and a forsterite-rich core. Some inclusions contain vesicles, indicating that they were once molten. The crystallization sequence inferred from textures is: spinel, forsterite, fassaite and, finally, Mg-rich melilite. One concentrically-zoned inclusion contains melilite in its mantle whose composition lies on the opposite side of the liquidus minimum in the melilite binary from that in its core. This suggests that segregation of forsterite from spinel in all of these inclusions could be due to volatilization of MgO and SiO₂ relative to Al₂O₃ and CaO from the outsides of droplets. CG-14 is relatively uniformly enriched in refractory elements relative to C1 chondrites by a factor similar to that for Ca-, Al-rich coarse-grained inclusions except for Ca, Al and Hf which are unusually low. No Ce anomaly such as found in FUN inclusions C1 and HAL is present in CG-14. Whole-rock samples of CG-14 and TE are more strongly mass-fractionated in oxygen relative to "normal" Allende inclusions than the FUN inclusion EK 1-4-1 and less so than C1. Relative to bulk Allende, both inclusions have strongly mass-fractionated magnesium and silicon and ²⁵Mg excesses or deficits of ²⁴Mg or ²⁶Mg. CG-14 has a ²⁹Si excess or a deficit of ²⁸Si or ³⁰Si. Volatilization loss cannot be responsible for the magnesium and silicon isotope fractionations, as this would require prohibitively large mass loss from these magnesium-rich inclusions. The remarkable similarity in textures between FUN and non-FUN inclusions implies similar thermal histories, arguing against different rates of evaporative loss of major elements. Sputtering alone may be insufficient to account for the magnitude and direction of oxygen isotope fractionation in FUN inclusions.

INTRODUCTION

A SMALL FRACTION of the refractory inclusions in Allende have unusual isotopic properties in oxygen, magnesium and silicon that led to the acronym FUN, indicating a combination of fractionation and unknown nuclear effects (CLAYTON and MAYEDA, 1977; WASSERBURG *et al.*, 1977). The fractionation consists of enrichments of the heavy isotopes of these elements by several permil per mass unit. The nuclear effects are either small deficiencies of ²⁴Mg or ²⁶Mg and ²⁸Si or ³⁰Si, or small excesses of ²⁵Mg and ²⁹Si. FUN inclusions lack the radiogenic ²⁶Mg found in the refractory inclusions in Allende. Two of these inclusions, C1 and EK 1-4-1, exhibit anomalies of nucleosynthetic origin in all elements studied (calcium, titanium, strontium, barium, neodymium, samarium). For a review, see LEE (1979). Inclusion HAL (LEE *et al.*, 1980) may belong to the FUN group, since it has strongly fractionated oxygen. However, its magnesium isotopes

are normal, and it contains too little silicon for a conventional isotopic analysis. HAL also has isotopically fractionated calcium (LEE *et al.*, 1979). Egg-3 has some, but not all, of the characteristics of FUN inclusions. It has mass-fractionated magnesium isotopes but also radiogenic ²⁶Mg (ESAT *et al.*, 1980); its silicon isotopes are not strongly fractionated but do have a ²⁹Si excess (MOLINI-VELSKO, 1983); its oxygen isotopes are not fractionated relative to typical Type B inclusions.

Because of the importance of FUN inclusions for revealing details of nucleosynthetic processes, it is desirable to find additional examples for analysis. Unfortunately, there are no known chemical, mineralogical, or textural characteristics which distinguish FUN inclusions as a group from other Allende inclusions, so that searches for more of them require isotopic analysis. All of the known FUN inclusions contain calcium-, aluminum-rich, magnesium-poor mineral assemblages (GRAY *et al.*, 1973; ALLEN *et al.*, 1980; NAGASAWA *et al.*, 1982) whose bulk compositions were established in high-temperature gas-condensed phase fractionation processes. Here, we describe and discuss the origin of two additional FUN inclusions that differ significantly from the above objects in being forsterite-rich and thus less refractory than previously described FUN inclusions.

⁵ Present address: Division of Geological and Planetary Sciences, California Institute of Technology, Pasadena, CA 91109.

ANALYTICAL TECHNIQUES

Petrographic and mineral analysis

Portions of one inclusion, CG-14, were found in two facing slabs cut from Allende. Material from the largest portion (~0.6 cm in maximum dimension) was dug from the slab and split for neutron activation and oxygen isotope analyses. Polished thin sections were made from the facing piece (~0.2 cm) and of two small chips dug from the largest portion. These were examined optically and with a JEOL JSM-35 scanning electron microscope, equipped with a KEVEX Si(Li) X-ray detector. Mineral analyses were obtained using an ARL-EMX-SM 3-spectrometer automated electron microprobe, operated at 15 keV accelerating voltage and 0.6 μ A beam current. Data were reduced via an on-line NOVA 2/10 computer, using the program MAGIC (J. W. Colby, Bell Laboratories). Natural and synthetic minerals and glasses were used as standards.

Petrographic and mineralogical studies of the other inclusion, TE, by DOMINIK *et al.* (1978), indicate striking similarity to CG-14. Because of this, the Chicago group requested a piece of TE from Dr. A. El Goresy for isotopic analysis in the hope that the latter would turn out to be another FUN inclusion. A 10 mg sample and two polished grain mounts of TE were made available for this purpose.

Major and trace element analysis

The chemical composition of a 37.42 mg sample of CG-14 was determined by instrumental neutron activation analysis (INAA). The sample was included in the same irradiations as the bulk sample of CG-11 analyzed by DAVIS *et al.* (1978), so the details of the procedure will not be repeated here.

Isotopic analysis

Oxygen and SiF₄ were extracted from whole-rock samples of CG-14 and TE using the bromine pentafluoride technique, with gas purification appropriate for O₂ analysis (CLAYTON and MAYEDA, 1983). Silicon tetrafluoride was separated from less volatile fluorides by distillation at -78°C. Further purification was effected by gas chromatography on a Teflon-lined column containing halocarbon oil 14-25 supported on Teflon (MOLINI-VELSKO, 1983). Oxygen isotope analyses were done on O₂⁺ ions for measurement of $\delta^{18}\text{O}$ and $\delta^{17}\text{O}$, using a 15-cm, 60° double-collecting mass spectrometer. Silicon isotope analyses were done on SiF₃⁺ ions for measurement of $\delta^{30}\text{Si}$ and $\delta^{29}\text{Si}$, using a 30-cm, 60° double-collecting mass spectrometer. Analytical uncertainties for oxygen and silicon are estimated 2 σ errors based on long-term measurements of reference samples.

The samples available were too small to permit mineral separation, which would be desirable to determine internal isotopic relationships within each inclusion. However, for TE, a crude chemical separation was achieved by carrying out the fluorination in two temperature steps. At the lower temperature (600°C), pyroxene should react preferentially, leaving mostly olivine and spinel for the second reaction at 730°C. A whole-rock analysis of TE was also done.

The Mg isotopic measurements were performed with a modified AEI IM-20 ion microprobe (BANNER and STIMPSON, 1975; STEELE *et al.*, 1977), largely following the procedures discussed by HUTCHEON (1982). Since only Mg-rich minerals were available for study, small primary beam currents (0.2–1 nA) were used, ensuring high spatial resolution (3–5 μ m). As discussed by Hutcheon, one limitation of ion probe Mg isotopic measurements is the degree of instrumental mass-fractionation, typically ± 7 permil/amu with the IM-20. Since the primary goal of this study was the investigation of intrinsic fractionation effects, new procedures were developed to minimize instrumental fractionation. Fragments, ~1 mm to 100 μ m in size, of the suspected FUN inclusions were mounted

in epoxy discs together with corresponding terrestrial minerals, *i.e.* spinel, olivine and diopside, plus fragments of normal Allende inclusions. By having isotopic standards and FUN material in the same mount it was possible to switch from one sample to the other in the ion probe with only minor shifts of the stage, without the need for refocussing the primary or secondary ion beams. By effectively eliminating the need for retuning, instrumental fractionation was reduced to less than ± 2 permil/amu for each set of analyses of a given standard. Analyses of Allende FUN samples were interspersed with analyses of standards of similar mineralogy. A typical run, for example, consisted of two or three analyses of terrestrial spinel, followed by Allende FUN spinel, followed by repeat analyses of the terrestrial spinel. Data were collected on each sample until the 2 σ mean errors in isotopic ratios were $< \pm 1\%$.

To test the capability of the Chicago ion probe to measure intrinsic fractionation effects, we measured the Mg isotopic composition of pyroxene from the Allende FUN inclusion Egg-3 previously studied by ESAT *et al.* (1979, 1980). Six individual pyroxenes were analyzed; all showed enrichments in ²⁵Mg and ²⁶Mg, yielding a mean fractionation of $6.7 \pm 2.2\%$ /amu, in excellent agreement with the results of ESAT *et al.* The data are not sufficiently precise to allow detection of any non-linear isotope effect. These results clearly demonstrate the capability to measure fractionation effects as small as 5‰/amu. Fractionation was calculated from the raw ²⁵Mg/²⁴Mg and ²⁶Mg/²⁴Mg ratios measured for CG-14 and TE relative to corresponding ratios measured in standards before and after. Isotopic ratios were corrected only for the measured system deadtime, 25 ± 2 ns; specifically, the normalization procedure discussed by HUTCHEON (1982) was not used.

Non-mass-dependent isotopic effects were calculated as $\delta_N^{25}\text{Mg}$ relative to ²⁵Mg/²⁴Mg = 0.12663 after correcting for mass-fractionation by normalizing to ²⁶Mg/²⁴Mg = 0.13938. Errors in individual isotopic ratios are $\pm 2\sigma$ mean as discussed by HUTCHEON (1982), while errors in fractionation were calculated using the 2 σ error of the mean for both FUN samples and standards.

The silicon isotopic composition of individual grains from CG-14 and TE was also measured with the ion probe, following the same techniques used for magnesium. The fractionation was again calculated relative to the isotopic composition of standards measured before and after, but the precision of the ion probe measurements is insufficient to detect the non-linear effect in ²⁹Si.

DESCRIPTIONS

CG-14 (Fig. 1) has an oblong shape and much of its exterior is angular, suggesting that it was broken prior to incorporation into Allende. Clastic rim material (MACPHERSON and GROSSMAN, 1981) mantles the outside and fills a round pocket in its interior. This pocket (Fig. 2) is probably a re-entrant in the third dimension and may be a vesicle (see Discussion).

Primary constituents of CG-14 are equant euhedral olivine (≤ 175 μ m) and spinel (≤ 40 μ m) crystals, both enclosed poikilitically within large fassaite pyroxene crystals (≤ 0.9 mm). Olivine and spinel are strongly segregated from one another, giving a very patchy appearance to the inclusion. Regions of fassaite containing coarse spinel grains have no olivine and those containing olivine have little spinel. In fact, some individual clinopyroxene crystals cross-cut spinel-rich and olivine-rich zones and contain only olivine inclusions at one end and only spinel at the other. Where olivine and spinel are in close proximity to one another, however, there is no evidence of any reaction relationship between them. Olivine crystals do, in many places, contain tiny (mostly ≤ 5 μ m; rarely up to ~ 15 μ m) rounded inclusions of spinel, bordering which are rare tiny (≤ 1 μ m) grains that may be perovskite. Occasionally, sharply pointed olivine crystal fragments project outward from the inclusion margin into the surrounding matrix. Thus, even locally, there is no smooth bounding surface

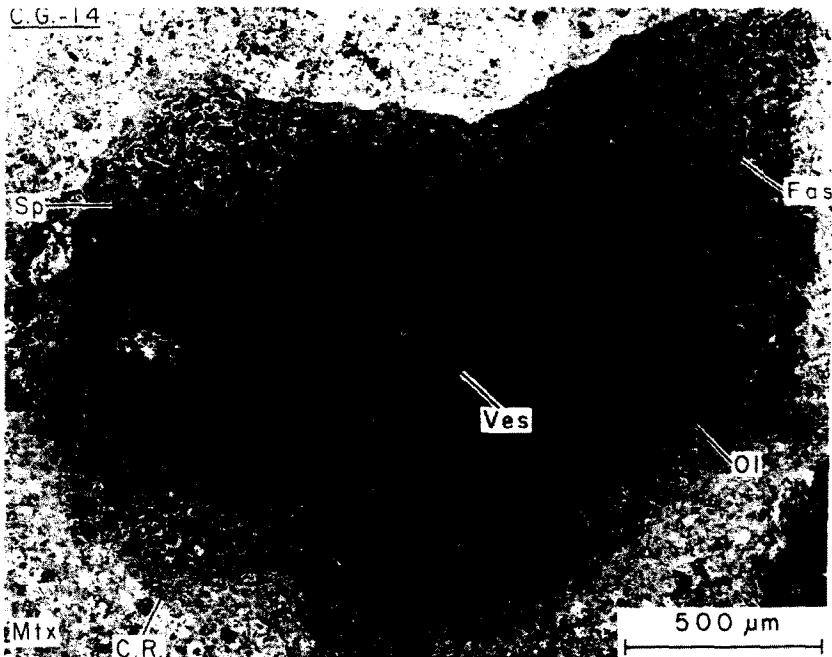


FIG. 1. Back-scattered electron photomicrograph of CG-14. Note its rugged margin, the patchy segregation of spinel (Sp) from olivine (Ol), the central vesicle (Ves) and the discontinuous mantle of clastic rim (C.R.) material that separates CG-14 from Allende matrix (Mtx). Fassaite (Fas; light grey) poikilitically encloses both spinel and olivine.

to the inclusion, further suggesting breakage prior to its incorporation into the matrix.

Occurring mostly near the margin of the inclusion and less abundantly in its interior are veins and patches of material that were modified by secondary processes (Fig. 3). These tend to be poor in fassaite and rich in olivine, the latter highly fractured and enriched in iron along fractures and grain mar-

gins, particularly near the edge of the inclusion (Fig. 1) and less so in its interior (Fig. 4). In these altered zones, areas between olivine crystals consist of nepheline, small iron-rich olivine crystals and void space. Secondary phases also occur in veins (Fig. 5) and in small cavities (Fig. 6), which are partially filled with wollastonite needles, diopside, hedenbergite and andradite. Spinel near alteration zones (Fig. 5) is generally

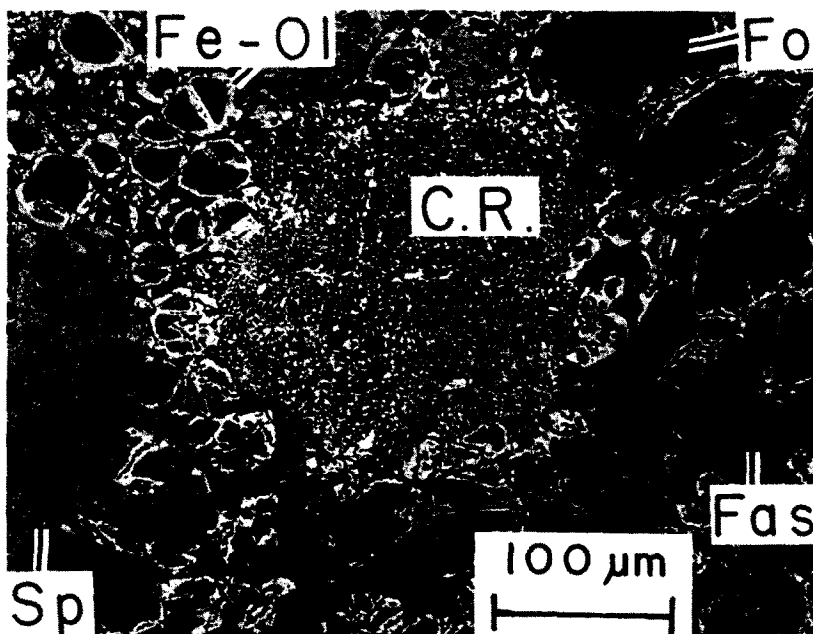


FIG. 2. Enlarged back-scattered electron image of the central vesicle in CG-14, showing that it is filled with clastic rim material. Abbreviations as in Fig. 1 except: Fo—forsteritic olivine; Fe-Ol—iron-rich olivine.

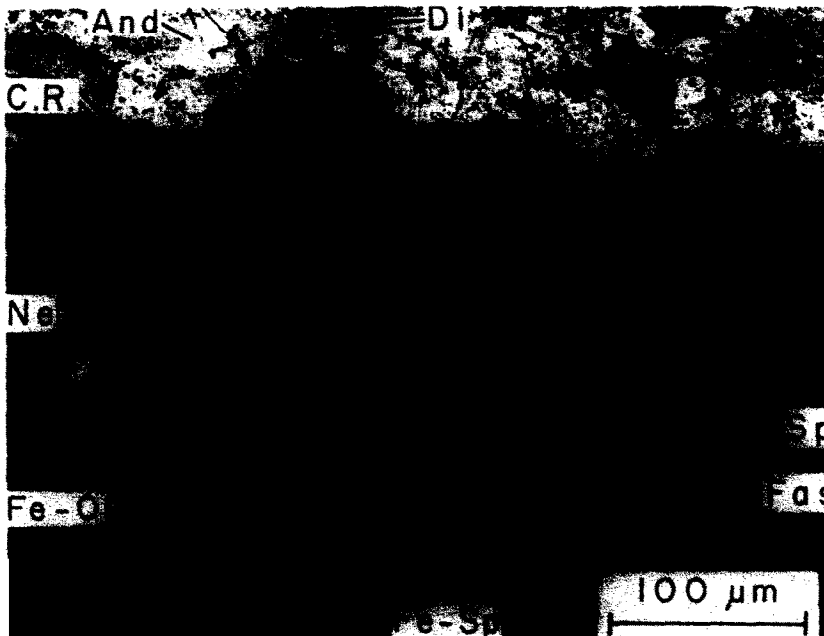


FIG. 3. Enlarged back-scattered electron image of part of the outer surface of CG-14, showing a spinel-rich area and an olivine-rich area. Separating the two is a porous alteration vein filled with iron-rich spinel (Fe-Sp), nepheline (Ne) and void space. Nepheline and iron-rich olivine also mantle forsterite crystals on the left. Clastic rim material mantles the outer surface of the inclusion (top) and consists of very fine-grained olivine and nepheline plus coarser diopside (Di) and andradite (And). Other abbreviations as in previous figures.

somewhat pink, reflecting enrichment in iron relative to colorless spinel elsewhere in the inclusion (see Mineral Chemistry), and is commonly rimmed by a thin layer of nepheline (Fig. 5). Individual fassaite crystals are weakly sector-zoned.

the sectors being distinguished optically by slight differences in birefringence and extinction angle. Near altered zones, pyroxene is enriched in iron (see Mineral Chemistry).

A rim sequence similar to the kind described by WARK

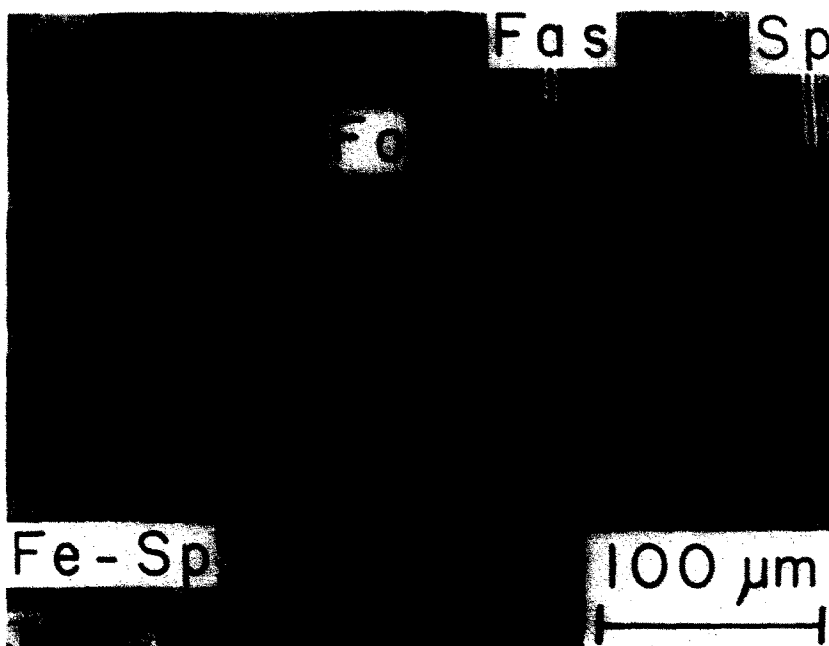


FIG. 4. Back-scattered electron image of a fragment from the interior of CG-14. Note the absence of iron-rich rims from forsterite crystals. There is no evidence of a reaction relationship between olivine and spinel. At bottom is an alteration zone in which the spinel is enriched in iron. Abbreviations as in previous figures.

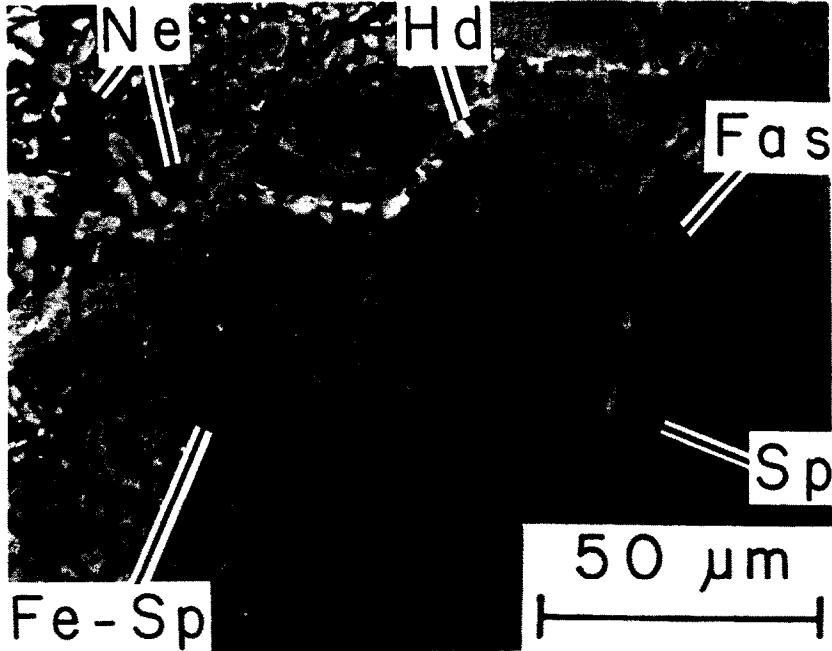


FIG. 5. Enlarged back-scattered electron image of part of CG-14, showing the gradual enrichment in iron in spinel with proximity to an altered zone (left; iron-rich spinel is lighter grey than iron-free spinel). Note the thin dark rim of nepheline around each iron-rich spinel grain. Nepheline also occupies interstices within the alteration zone. A tiny vein is partly filled with hedenbergite (Hd; bright). Other abbreviations as in previous figures.

and LOVERING (1977) is only locally present in CG-14, supporting the idea that the inclusion was broken prior to incorporation into the Allende parent body. Where present, the rim consists of a poorly defined layer of olivine + nepheline, one of diopside, and an outermost mantle of andradite and

pyroxene, the latter ranging in composition from diopside (needle-like) to hedenbergite (massive aggregates). Unlike rim sequences on other Allende refractory inclusions, there are no layers on CG-14 containing anorthite, grossular, spinel or perovskite.

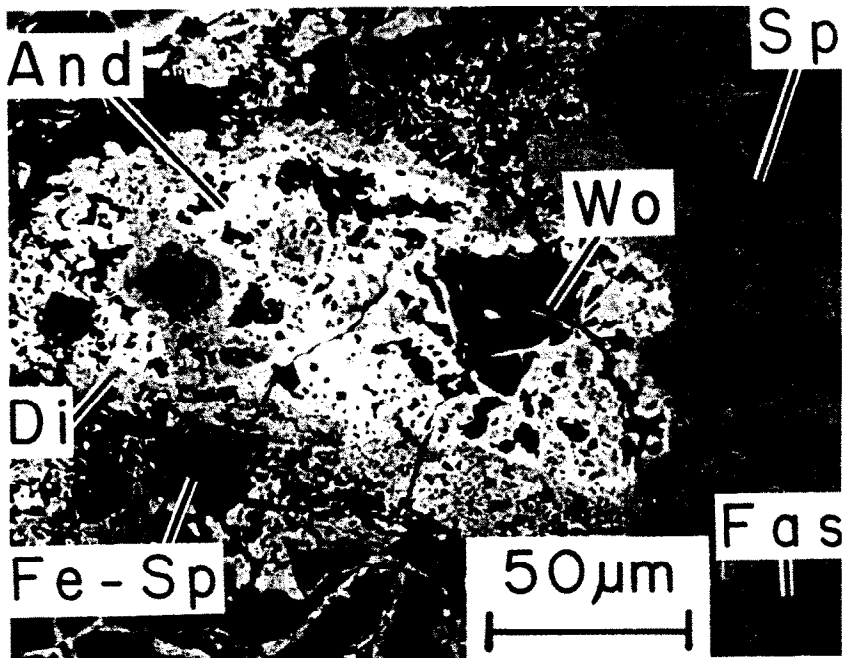


FIG. 6. Enlarged back-scattered electron image of a cavity in CG-14 that is partially filled with andradite, diopside and needles of wollastonite (Wo). Other abbreviations as in previous figures.

CG-14 is very similar in mineralogy and texture to four other forsterite-, fassaite-, spinel-bearing inclusions, bringing to five the number of known objects belonging to this class. Two, CG-14 and TE, are now known to possess unusual isotopic characteristics, two do not and the fifth has not been isotopically analyzed. TE was described in detail by DOMINIK *et al.* (1978) and differs from CG-14 in several respects. Spinel is concentrated near the margin of TE and in pockets extending from the margin toward the core. TE thus has an apparent concentric zonation, with olivine being present mostly in the core and spinel mostly in the mantle. CG-14, in contrast, has a patchy distribution of spinel and olivine, and shows no evidence of concentric structure. TE contains several grains of anorthite and åkermanite-rich ($\text{Åk} \sim 88$) melilite in its spinel-rich outer zone, which have not been found in CG-14. TE also has veins of a potassium-rich "layer structure" phase that replaces fassaite. Such a phase has not been found in CG-14. Finally, TE does not show replacement of forsterite by iron-rich olivine like that in CG-14.

A third forsterite-bearing inclusion in our collection, Al6S3, is illustrated in its entirety in Fig. 5 of CLAYTON *et al.* (1977). Like TE, Al6S3 has a concentric zoned structure. Its core contains mostly euhedral olivine crystals enclosed poikilitically within fassaite. A few spinel-rich areas are also present, as well as extremely rare crystals of åkermanite-rich ($\text{Åk} \sim 80$) melilite. Spinel crystals generally occur in convoluted chains that, in many places, enclose clinopyroxene grains. Much smaller spinel grains occur as inclusions within olivine. Spinel-pyroxene assemblages are mostly confined to the margin of the inclusion but they do not form a continuous mantle around Al6S3. Rather, they occur as discrete regions, separated from one another by olivine-, pyroxene-rich regions or by secondary minerals. Where the surface of the inclusion is unbroken, marked by an intact Wark-Lovering rim, spinel-pyroxene regions are always closer to the margin than olivine-pyroxene ones. The outermost 100–200 μm zone is highly altered, but numerous primary crystals of aluminous melilite ($\text{Åk} 20\text{--}43$) and anorthite can be seen. The fourth forsterite-bearing inclusion, ALVIN, is illustrated in its entirety by MACPHERSON *et al.* (1981). In this inclusion, spinel crystals are concentrated into irregular patches which are also rich in alteration products, but the inclusion is not concentrically zoned. No iron-rich olivine was found, but a Wark-Lovering rim is present. ALVIN is noteworthy in containing numerous spheroidal voids in its interior, each lined with wollastonite needles. These voids are probably vesicles which, together with the spheroidal shape of the inclusion itself and its poikilitic textures, leave little doubt that the inclusion was once a molten droplet. Al6S3 (CLAYTON *et al.*, 1977) and ALVIN (unpublished data) are not FUN inclusions.

Finally, BLANDER and FUCHS (1975) described an inclusion, 9/16, that is similar in mineralogy and texture to the four noted above. Those authors do not note any concentric zonation and, judging from their Fig. 8, olivine and spinel are not significantly segregated from one another. Anorthite and åkermanite-rich melilite (of bimodal composition, $\text{Åk} 66\text{--}67$ and $\text{Åk} 87\text{--}88$) are present in minor amounts, but no mention is made of whether or not these phases occur preferentially in the outer parts of 9/16. The isotopic composition of this inclusion is unknown.

MINERAL CHEMISTRY

Olivine

Primary olivine in CG-14 is nearly pure forsterite (Table 1) whose chief minor component is calcium (up to 2.07 wt.%). FeO in the cores of olivine crystals is very low near the center of the inclusion (≤ 0.4 wt.% FeO; Table 1, #1) and increases slightly towards the margin of the inclusion (0.13–0.14 wt.% FeO; Table 1, #2). Rims of olivine crystals near alteration zones are FeO-rich (over 3 wt.% FeO; Table 1, #3), especially so on those near the inclusion margin (up to 27 wt.% FeO).

TABLE 1
Electron microprobe analyses
of olivine in CG-14

	1	2	3
SiO ₂	43.96	43.27	42.97
Al ₂ O ₃	.16	.16	.21
MgO	54.48	54.86	52.86
CaO	1.59	1.70	1.80
FeO	<.03	.14	3.12
Total	100.19	100.13	100.96
Cations per 4 oxygens			
Si	1.027	1.015	1.015
Al	.004	.004	.006
Mg	1.898	1.918	1.858
Fe	.000	.003	.061
Ca	.040	.043	.046
Total	2.969	2.983	2.984

(1) crystal core, near center of CG-14; (2) crystal core, near margin of CG-14; (3) near fracture, in alteration zone.

All analyses by wavelength dispersion
Detection limit (3σ) for Fe is
 ~ 0.03 wt.% FeO

All olivine contains low but consistent amounts of Al₂O₃ (0.09–0.16 wt.%). Calcium contents of olivine in CG-14 are comparable to those in Al6S3 (1–1.4 wt.% CaO), but lower than the highest in TE, ~ 11 wt.% (DOMINIK *et al.*, 1978). Iron contents of olivine in TE, < 0.05 wt.% (DOMINIK *et al.*, 1978), and in 9/16, ~ 0.2 wt.% (BLANDER and FUCHS, 1975), are comparable to those of many in CG-14 but less than the highest concentrations found in altered olivine in CG-14.

Pyroxene

Pyroxene in CG-14 is sector-zoned fassaite and has a wide range of Al and Ti contents similar to the ranges reported by DOMINIK *et al.* (1978) in TE, by BLANDER and FUCHS (1975) in 9/16, and in Al6S3. Analyses of Ti-, Al-rich and Ti-, Al-poor varieties are given in Table 2. The iron content of pyroxene is 0.03–0.16% in crystals near the inclusion center and far from altered zones. The highest iron contents are slightly higher than those reported by DOMINIK *et al.* (1978) in TE. Near the margin of CG-14 and its interior alteration zones, pyroxene is enriched in FeO up to ~ 4 wt.%.

Spinel

Most spinel in CG-14 is nearly pure MgAl₂O₄. Spinel far from alteration zones has 0.85–1.77% FeO, 0.14–0.18% CaO, 0.19–0.20% TiO₂, 0.12–0.14% SiO₂ and 0.04–0.07% V₂O₅. Spinel near alteration zones has up to 13% FeO, 0.11% CaO, 0.15% TiO₂, 0.22% SiO₂ and 0.09% V₂O₅. Minor element contents of one spinel in TE reported by DOMINIK *et al.* (1978) are generally similar to those in spinel far from alteration zones in CG-14, the major difference being the much lower FeO content in TE spinel, 0.01 wt.%. Dominik *et al.* saw no composition differences between spinel crystals from the core and rim of TE.

Detection limits for minor elements in spinel are (3σ): V₂O₅—0.01 wt.%; FeO—0.02 wt.%; CaO—0.02 wt.%; SiO₂—0.02 wt.%; TiO₂—0.03 wt.%.

BULK COMPOSITION

In order to determine if the portion of CG-14 taken for INAA (Table 3) is representative of the bulk in-

TABLE 2
Electron microprobe analyses
of clinopyroxene in CG-14

	1	2	3
SiO ₂	42.29	44.62	47.23
TiO ₂ *	4.24	3.84	2.36
Al ₂ O ₃	17.33	15.76	11.70
MgO	11.97	12.66	14.18
CaO	23.96	22.68	22.74
FeO	.16	.10	.18
Total	99.95	99.66	98.39
Cations per 6 oxygens			
z			
Si	1.536	1.612	1.725
Al	.464	.388	.275
M1			
Al	.278	.283	.228
Mg	.601	.610	.703
Fe	.005	.003	.005
Ti*	.116	.104	.064
M2			
Ca	.932	.878	.890
Mg	.047	.072	.068
Total	3.979	3.950	3.958

*All Ti as Ti⁴⁺
All analyses by wavelength
dispersion
Detection limit (3σ) for Fe is
~0.03 wt. % FeO

Table 3. Major and trace element abundances¹ in CG-14.

Element	Concentration	Enrichment factor relative to CI chondrites ²
Na ₂ O	3733 ± 5	0.563
MgO	35.99 ± .89%	2.28
Al ₂ O ₃	16.78 ± .14%	10.6
SiO ₂ ³	33.08 ± 1.05%	1.46
CaO	10.03 ± .54%	7.97
TiO ₂	1.210 ± .086%	17.0
FeO	2.481 ± .027%	0.105
Sc	113.8 ± .3	20.0
V	71.6 ± 5.2	1.29
Cr	539.4 ± 6.3	0.207
Mn	208 ± 3	0.110
Co	4.50 ± .27	0.00891
Ni	.79	<0.0073
Ru	11.49 ± .94	16.1
La	3.193 ± .042	13.3
Ce	8.44 ± .65	13.8
Sm	2.072 ± .008	14.2
Eu	0.720 ± .010	13.1
Tb	0.40 ± .12	11.1
Dy	4.51 ± .23	18.8
Yb	2.524 ± .060	15.9
Lu	0.365 ± .011	15.3
Hf	0.472 ± .095	3.73
Os	7.09 ± .11	14.1
Ir	5.823 ± .015	12.5
Au	7.8 ± 1.2 ppb	0.0526

¹Concentrations are in ppm unless otherwise indicated. The uncertainties given are 1σ error bounds based on counting statistics alone. Additional uncertainties due to uncorrected variations in neutron fluence and counting geometry are estimated to be less than 3%.

²CI chondrite abundances used are essentially the same as in Davis *et al.* (1982).

³Determined by difference.

clusion as seen in thin section, its modal mineralogy was calculated from the bulk chemical analysis and the chemical compositions of the minerals present. Major minerals found in the petrographic examination of CG-14 are olivine, fassaite and spinel. Assuming that these are the only minerals present, the mineralogy was calculated from the mass balance equations for MgO, Al₂O₃ and CaO. The analyses used for olivine and pyroxene were analyses 1 from Table 1 and 2 from Table 2. Spinel was assumed to be stoichiometric MgAl₂O₄ with the addition of the minor elements given in the Mineral Chemistry section. We calculate that CG-14 contains 45 wt.% olivine, 38 wt.% fassaite and 15 wt.% spinel, in good agreement with the proportions estimated in thin section. In order to check this calculation, we computed SiO₂, TiO₂ and FeO contents from the mineral chemistry and these mineral proportions. We found 36.6% SiO₂, 1.48% TiO₂ and 0.25% FeO. These values can be compared with the measured bulk composition in Table 3. The reason for the discrepancy in SiO₂ is not known, but it should be noted that SiO₂ was determined by difference and is sensitive to errors in the analyses of other elements. The calculated TiO₂ content is in good agreement with the measured value. The reason for the discrepancy in FeO is that iron-rich olivine and alteration phases were not included in the mineralogy calculation.

CG-14 is enriched in both lithophile and siderophile refractory trace elements, with these elements having a mean enrichment factor of 15.0 ± 7 relative to CI chondrites. The mean enrichment factor in nine coarse-

grained inclusions (GROSSMAN *et al.*, 1977), 17.5 ± .4, is only slightly higher than that of CG-14. The only anomalous refractory element in CG-14 is hafnium, which has an enrichment factor of only 3.7. The refractory element enrichment pattern of CG-14 (Fig. 7) may seem irregular, but it is not less uniform than those of individual normal coarse-grained inclusions.

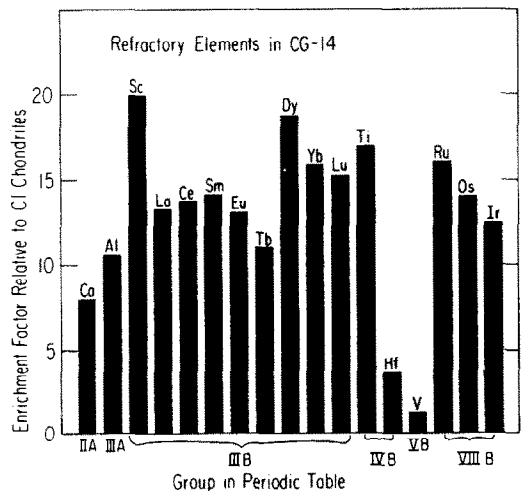


FIG. 7. Enrichment factors for refractory elements in CG-14 relative to CI chondrites are like those in Allende coarse-grained inclusions, except for Ca, Al and Hf which are unusually low.

Table 4. Mass Spectrometric Determinations of Oxygen and Silicon Isotopic Compositions of Inclusions CG-14 and TF

		$\delta^{18}\text{O}$ (‰ rel. SMOW)	$\delta^{30}\text{Si}$ (‰ rel. NBS28)	$\delta^{34}\text{S}$ (‰ rel. NBS28)
CG-14	w.r.	-11.04	-12.16	+11.67
TF	w.r.	-4.21	-15.73	+11.91
	w.r. 600	-0.74	-8.04	+10.25
	w.r. 730	-6.79	-19.34	+11.17

2 σ errors are ± 0.15 of all data, based on replicate analyses of standards.

ISOTOPIC COMPOSITION

Analytical data for oxygen, silicon and magnesium (Tables 4 and 5) show the FUN characteristics previously observed in C1 and EK 1-4-1: oxygen isotopes displaced toward heavy-isotope enrichment relative to "normal" Allende inclusions, strongly mass-fractionated magnesium and silicon and, in some cases, excess ^{25}Mg and ^{29}Si .

The oxygen isotope data are plotted in Fig. 8, which also includes the analyses of three other FUN inclusions. The three data points for TE fall on a line which converges at the upper end with the mixing lines for other FUN and "normal" inclusions. A similar convergent line has been drawn through the single analysis of CG-14. (By the time the anomalous nature of CG-14 was discovered, the remainder of the inclusion had been used up in other studies, so that it was not possible to analyze separated minerals.) These patterns have been interpreted as the outcome of two successive processes: (1) a mass-dependent heavy isotope enrichment along the slope-1/2 line beginning at the lower left, and extending to a different degree for each inclusion, followed by (2) exchange of the phases in the inclusion with an external (probably gaseous) oxygen-bearing reservoir (CLAYTON and MAYEDA, 1977). The extent

of this exchange was least for spinel and greatest for melilite.

The magnesium isotopic composition of olivine, pyroxene and spinel from CG-14, olivine and spinel from TE, and the corresponding terrestrial minerals was measured with the ion probe. No phases with high Al/Mg ratio were located in either inclusion. The results of these measurements are summarized in Table 5 and Figs. 9 and 10. The solid line in the Mg three-isotope diagrams, Figs. 9 and 10, is a slope one-half line corresponding to linear mass-fractionation normalized to the data from terrestrial samples. The magnesium isotopic compositions of CG-14 and TE samples are clearly related to normal magnesium by linear mass-fractionation. All of the samples from CG-14 and TE are substantially enriched in both ^{25}Mg and ^{26}Mg relative to ^{24}Mg . The magnesium isotopic composition of both terrestrial and Allende FUN spinel is fractionated by $\sim 2.5\text{‰/amu}$ favoring the heavy isotopes relative to terrestrial and Allende olivine, respectively. This systematic shift is a consequence of secondary ion production by ion sputtering and, since the magnitude of the shift is the same for both normal and FUN samples, does not affect the measurement of intrinsic fractionation. The magnitude of the mass-fractionation in TE and CG-14 calculated by comparing the magnesium isotopic composition of any pair of Allende and terrestrial minerals analyzed sequentially is the same: $12.6 \pm 1.2\text{‰/amu}$ for TE and $17.5 \pm 1.4\text{‰/amu}$ for CG-14.

As shown in Figs. 9 and 10, the data from TE and especially from CG-14 lie somewhat above the linear fractionation line, suggesting a small non-mass-dependent isotopic effect in addition to the large fractionation. After correcting for fractionation by normalizing to $^{26}\text{Mg}/^{24}\text{Mg} = 0.13938$, the residual en-

Table 5. Ion Microprobe Determinations of Magnesium and Silicon Isotopic Compositions of CG-14, TE and Egg-3

SAMPLE	Unnormalized, Relative to Terrestrial Standards (‰) ¹				Normalized (‰) ²	
	$\delta^{25}\text{Mg}$	$\delta^{26}\text{Mg}$	$\delta^{30}\text{Si}$	$\delta^{30}\text{Si}$	$\delta^{25}\text{Mg}$	$\delta^{29}\text{Si}$
CG-14						
Olivine 1	19.0 \pm 1.1	34.0 \pm 1.1	6.1 \pm 2.6	11.1 \pm 2.8	2.0 \pm 1.7	0.6 \pm 1.4
Olivine 2	17.4 \pm 1.5	31.7 \pm 1.4	4.6 \pm 2.7	12.0 \pm 3.0	0.6 \pm 2.0	-1.4 \pm 3.7
Olivine 3	19.2 \pm 1.4	36.8 \pm 1.8	5.3 \pm 2.0	10.1 \pm 2.3	0.8 \pm 2.2	0.3 \pm 4.0
Pyroxene 1	17.3 \pm 1.3	35.2 \pm 1.6			-0.3 \pm 1.8	
Pyroxene 2	18.8 \pm 1.5	35.8 \pm 1.4	8.4 \pm 2.1	15.8 \pm 2.8	0.9 \pm 2.0	0.5 \pm 3.5
Spinel 1	19.0 \pm 1.2	34.6 \pm 1.4			1.8 \pm 1.8	
Spinel 2	16.5 \pm 1.2	33.2 \pm 1.4			0.2 \pm 1.8	
Spinel 3	19.6 \pm 1.5	38.0 \pm 1.6			0.6 \pm 2.1	
Spinel 4	18.0 \pm 1.4	34.0 \pm 1.8			1.0 \pm 2.2	
				Mean	0.9 \pm 0.7	
TE						
Olivine 1	12.5 \pm 1.6	26.0 \pm 1.5			-0.4 \pm 2.1	
Olivine 2	13.5 \pm 1.5	24.8 \pm 1.6			1.1 \pm 2.1	
Olivine 3	13.5 \pm 1.8	26.4 \pm 1.8	3.5 \pm 2.6	7.6 \pm 2.8	0.3 \pm 2.5	-0.3 \pm 3.5
Olivine 4	11.9 \pm 1.8	25.4 \pm 1.8			0.8 \pm 2.5	
Spinel 1	12.7 \pm 1.4	23.5 \pm 1.7			1.0 \pm 2.2	
Spinel 2	13.0 \pm 1.5	25.2 \pm 1.8			1.5 \pm 2.3	
				Mean	0.8 \pm 0.6	
Egg-3						
Pyroxene 1	8.8 \pm 1.7	15.8 \pm 1.9			0.9 \pm 2.5	
Pyroxene 2	7.0 \pm 1.6	13.7 \pm 1.6	-1.1 \pm 2.1	-1.8 \pm 2.4	0.2 \pm 2.2	0.2 \pm 3.0
Pyroxene 3	7.5 \pm 1.6	14.0 \pm 1.7			0.5 \pm 2.3	
Pyroxene 4	4.4 \pm 1.7	9.4 \pm 1.9			-0.3 \pm 2.5	
Pyroxene 5	6.4 \pm 1.8	13.7 \pm 2.0			-0.4 \pm 2.8	
				Mean	0.2 \pm 0.4	

¹ δ -values calculated relative to isotopic composition of standards analyzed before and after (see text).

²Normalized to $^{26}\text{Mg}/^{24}\text{Mg} = 0.13938$; $^{30}\text{Si}/^{28}\text{Si} = 0.03163$.

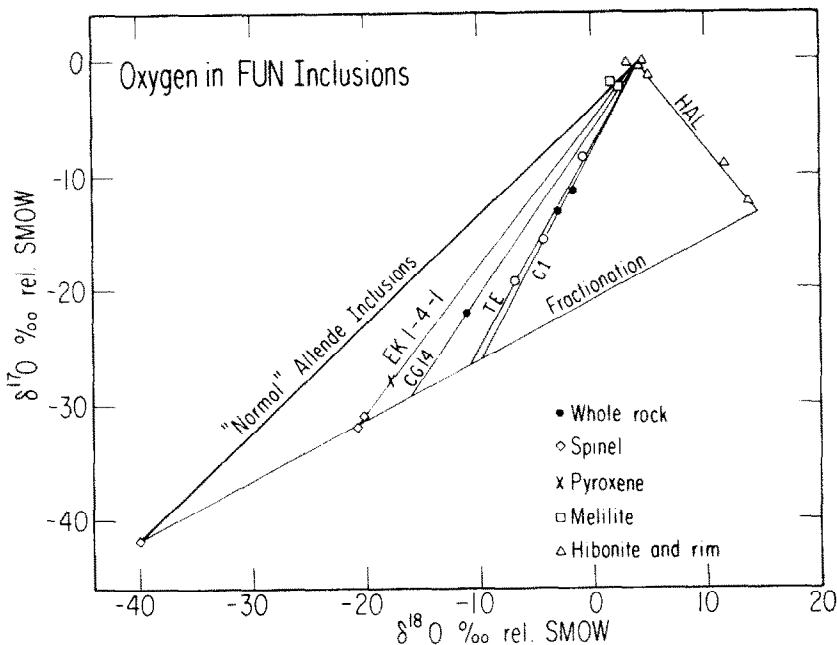


FIG. 8. Three-isotope graph for oxygen in FUN inclusions. The line labelled "Normal Allende Inclusions" is the locus of data points from inclusions and separated minerals from about 95% of the Allende CAI. The FUN inclusions appear to have acquired their compositions in two stages: first, a mass-dependent fractionation, moving to the right along the line labelled "Fractionation", then exchange with a common external reservoir to produce the lines converging to a common composition at the top of the graph. Data for TE are shown as open circles (see Table 4).

richment in ²⁵Mg is $\delta_N^{25}\text{Mg} = 0.8 \pm 0.6\text{‰}$ for TE and $\delta_N^{25}\text{Mg} = 0.9 \pm 0.7\text{‰}$ for CG-14. These ²⁵Mg enrichments are similar in magnitude to the non-mass-dependent isotopic effects measured in CI and EK 1-4-1 (WASSERBURG *et al.*, 1977).

All individual samples from both CG-14 and TE exhibit uniform Mg isotopic composition, from grain to grain and mineral to mineral as well as within single grains on a 5 μm spatial scale. Isotopic homogeneity is observed both for the large mass-dependent frac-

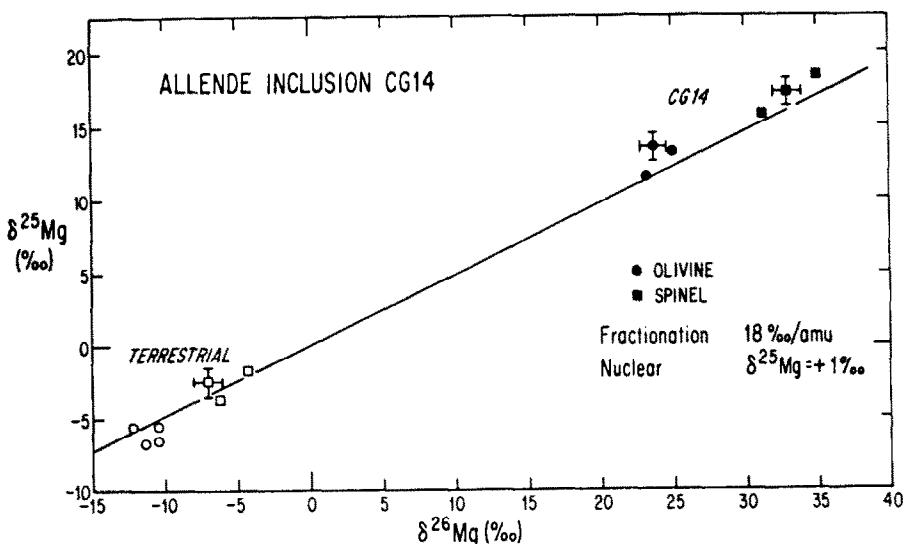


FIG. 9. Magnesium isotopic data obtained by ion microprobe for olivine and spinel from CG-14 and from terrestrial olivine and spinel. The solid line has a slope of one-half. Magnesium in CG-14 is mass-fractionated relative to normal magnesium and has excess ²⁵Mg or a deficit of ²⁶Mg or ²⁴Mg. δ values calculated relative to $^{25}\text{Mg}/^{24}\text{Mg} = 0.12663$, $^{26}\text{Mg}/^{24}\text{Mg} = 0.13938$. Measurement errors are the same for all data points. To avoid confusion, error bars are only shown for three points.

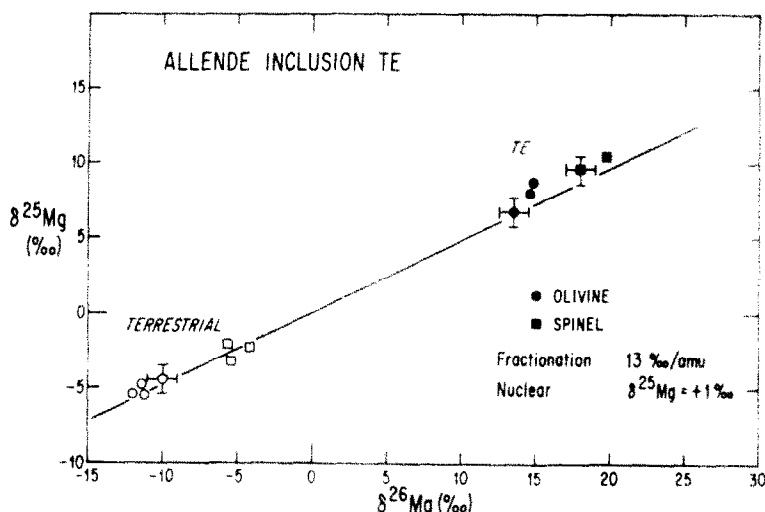


FIG. 10. Magnesium isotopic data obtained by ion microprobe for olivine and spinel from TE and from terrestrial olivine and spinel. The solid line has a slope of one-half. Magnesium in TE is mass-fractionated relative to normal magnesium and has excess ^{25}Mg or a deficit of ^{26}Mg or ^{24}Mg . δ values calculated relative to $^{25}\text{Mg}/^{24}\text{Mg} = 0.12663$, $^{26}\text{Mg}/^{24}\text{Mg} = 0.13938$. Measurement errors are the same for all data points. To avoid confusion, error bars are only shown for three points.

tionation and for the small non-mass-dependent enrichment in ^{25}Mg present after normalization. Similar behavior was also observed for samples from FUN inclusion C1 in another ion probe study (HUNEKE *et al.*, 1983). The uniform isotopic composition can be used to set limits on the post-crystallization history of CG-14. An iron-rich spinel located at the periphery of a cavity had a magnesium isotopic composition indistinguishable from that of normal, iron-poor spinel. If FeO were introduced into the inclusion and taken up by spinel during a low temperature secondary event, that process did not alter the magnesium isotopic composition of spinel.

Silicon isotopic compositions were determined by conventional mass spectrometry on bulk samples and by ion probe on individual minerals. The former has higher precision, the latter higher spatial resolution. Table 4 shows that the mass-dependent fractionation of silicon, relative to bulk Allende ($\delta^{30}\text{Si} = -0.70\text{‰}$, $\delta^{29}\text{Si} = -0.35\text{‰}$) is 7.3‰/mass unit in CG-14 and 6.3‰/mass unit for TE. Some internal fractionation is also evident between the two components of TE. CG-14 has an apparent excess of ^{29}Si of 0.3‰ (or a corresponding deficiency of ^{28}Si or ^{30}Si). No departure from a mass-fractionation line was found for TE. EK 1-4-1 has a 1.2‰ excess of ^{29}Si , and C1 has an excess of 0.4‰ (MOLINI-VELSKO *et al.*, 1983).

Ion probe measurements of the silicon isotopic composition of olivine and pyroxene from CG-14 and olivine from TE show that, like magnesium, silicon is related to normal silicon by linear mass-fractionation favoring the heavy isotopes. The ion probe measurements show that silicon in CG-14 olivine is fractionated by $6.1 \pm 2.5\text{‰/amu}$ relative to normal silicon, in good agreement with the bulk silicon isotopic analyses by conventional mass spectrometry. The precision of the

ion probe measurements is inadequate to detect the small enrichment in ^{29}Si . The ion probe measurements demonstrate that the isotopic composition of silicon, like that of magnesium, is uniform both among the primary phases and within individual grains on a scale of $\sim 5 \mu\text{m}$.

DISCUSSION

Forsterite-, spinel-, fassaite-bearing inclusions such as CG-14 are much rarer than Types A and B inclusions (GROSSMAN, 1975). At least two of the five such objects now known (CG-14 and TE) have unusual isotopic characteristics. Yet, in spite of their isotopic peculiarities, CG-14 and TE are petrographically very similar to the other forsterite-, spinel-, fassaite-bearing inclusions. These inclusions thus pose the same sort of problem as other FUN inclusions because, except for their isotopic anomalies, they are indistinguishable from "normal" inclusions of the same type.

CG-14 and TE are important for two other reasons. First, their existence indicates that FUN isotopic properties are not restricted to refractory bulk compositions, since these forsterite-bearing inclusions are far more Mg-, Si-rich than the Type B FUN inclusions and HAL. Second, at least two out of five known forsterite-bearing inclusions are FUN, a high proportion relative to FUN Type B's.

Petrologic constraints on the origin of CG-14 and TE

The textures, modal mineralogy and mineral chemistry of CG-14 are so similar to those of the other forsterite-bearing inclusions that they must all have had similar thermal histories. The inclusion ALVIN

was almost certainly once molten, as indicated by its vesicular nature and spheroidal shape. The cavity in CG-14 (Fig. 1), now filled by clastic rim material, is probably also a vesicle that was "frozen" in the act of escaping from the droplet, like the large vesicle in ALVIN (see Fig. 5a of MACPHERSON *et al.*, 1981). There is no indication of vesicular structure in TE (DOMINIK *et al.*, 1978) or in 9/16 (BLANDER and FUCHS, 1975) and only a slight hint of a vesicle in Al6S3. One feature shared by all five inclusions is the high calcium content of the olivine. WARNER and LUTH (1973) studied solubility relationships along the join monticellite (CaMgSiO_4)-forsterite. Their results indicate that, at low pressure, 4–5 mole % monticellite, the amount present in CG-14, is soluble in forsterite only at temperatures in excess of 1000°C. A monticellite content in excess of 20 mole %, the amount present in some olivine in TE, is soluble in forsterite only at temperatures greater than 1400°C. Below these temperatures, the solid solutions are unstable relative to the two-phase assemblage: forsterite solid solution + monticellite solid solution. It is important to note that since no monticellite-rich phase was found coexisting with the forsterite-rich one in these inclusions, the temperatures indicated are lower limits to the final equilibration temperatures. This assumes that the experimental data for the pure binary are directly applicable to the bulk composition of CG-14. Because the solidus temperatures for these forsterite-, spinel-, fassaite-bearing objects are in the range 1200–1250°C (STOLPER, 1982), we conclude that TE was once at least partially molten. Taking all of the evidence together, it is probable that all five of these objects were once at least partially molten.

The occurrences of spinel within olivine in CG-14 and the other inclusions, and of olivine within fassaite, indicate that the crystallization sequence was spinel before olivine before pyroxene. Because spinel was the first phase to crystallize, the bulk compositions of these inclusions can be plotted as projections from spinel onto the plane forsterite-anorthite-gehlenite (STOLPER, 1982). Plotted in this manner, the bulk composition of CG-14 (Table 3) indicates that the equilibrium crystallization sequence should be spinel, spinel + olivine, spinel + olivine + melilite, spinel + olivine + melilite + pyroxene. The problem is that melilite is absent from some of these inclusions and, in those in which it occurs, it is not enclosed within pyroxene but instead is interstitial. Thus, although textures in the inclusions are in accord with the crystallization sequence of spinel, olivine and pyroxene predicted from liquid-solid phase equilibria, melilite appears to be out of order, possibly due to kinetics. Dynamic crystallization experiments on liquids of Allende Type B bulk composition show that crystallization temperatures of plagioclase and melilite are strongly dependent on cooling rate and maximum temperature (MACPHERSON *et al.*, 1983; PAQUE and STOLPER, 1983) and that these factors played an important role in the crystallization history of actual Type B inclusions. It is thus reasonable to

assume that kinetics could have delayed the appearance of melilite in these forsterite-bearing objects as well.

The most curious feature in these objects is their textural heterogeneity, particularly the segregation of spinel from olivine. Although spinel grains in Type B refractory inclusions do show a tendency to clump together, they do not show a marked antipathy for any other phase like that in forsterite-bearing inclusions. One obvious possible explanation is that a reaction relationship exists between olivine and spinel. There is, however, no textural or experimental evidence for that. Places can be found in CG-14 and other inclusions where euhedral olivine and spinel crystals sit side by side with no hint of any reaction between them.

Another possibility is crystallization of a liquid droplet that became heterogeneous in composition due to intense volatilization from its outer surface. Such a process would lead to loss of silicon and magnesium relative to aluminum and calcium from the outside of the droplet. Evidence that this might have occurred comes from the concentric zonation of TE and Al6S3. The outer parts of TE are spinel-rich and the interior forsterite-rich. The outer zones of Al6S3 are composed of spinel, anorthite and gehlenite-rich melilite, but olivine and åkermanite-rich melilite constitute its interior. The dichotomy of melilite composition in Al6S3 is particularly significant because the compositions lie on opposite sides of the liquidus minimum in the binary system gehlenite-åkermanite. The composition of the minimum (Åk73) does not change significantly with additional components (GEE and OSBORN, 1969). Thus the two melilite compositions in Al6S3 *cannot have been derived by fractional crystallization of a single homogeneous liquid*. If volatilization is the mechanism that led to segregation of spinel from olivine, CG-14 and other inclusions not showing concentric zonation might be explained by breakage and rafting of the partly solidified spinel-rich mantle while the olivine-rich interior was still molten. The phenomenon whereby individual pyroxene crystals enclose only spinel at one end and only forsterite at the other in CG-14 could have resulted from initial pyroxene crystallization around spinel in the outer margins and continuation of pyroxene growth after rafting of spinel-rich pieces into the forsterite-rich interior had occurred.

One other possibility is that either spinel-rich fragments were incorporated as xenoliths into olivine-rich melts or *vice versa*. Such a process could account for the patchwork structure of CG-14 but could not explain the concentric structure of TE and Al6S3. Although the evidence is not conclusive, we believe that the volatilization model can better explain the observed features in all of these inclusions.

Chemical constraints on the origin of CG-14 and TE

A model that is usually invoked to explain inclusions which are relatively uniformly enriched in refractory

elements relative to C1 chondrites but to a lesser degree than are coarse-grained inclusions involves accretion of the inclusions from a mixture of refractory condensate precursors with less refractory magnesium silicates. An interesting feature of CG-14, however, is that the enrichment factors for the refractory major elements aluminum and calcium are substantially less than those of refractory lithophile trace elements. The implication is that the refractory condensate precursor assemblage for CG-14 was enhanced in trace elements relative to major elements compared to Allende coarse-grained inclusions. This is possible only if a large fraction of each of the trace refractory lithophiles is present in minor or trace phases which are separable from the major phases that carry most of the calcium and aluminum. Perovskite is an excellent candidate for the trace element carrier since titanium has an enrichment factor of 17.0, comparable to those of the trace refractory lithophiles.

Two of the other three FUN inclusions whose trace element compositions are known, C1, EK 1-4-1 and HAL, have unusual trace element patterns. C1 (CONARD, 1976) and HAL (DAVIS *et al.*, 1982) both show evidence of gas-solid fractionation under oxidizing conditions, since they are depleted in cerium and vanadium, but the trace element characteristics of EK 1-4-1 (NAGASAWA *et al.*, 1982) are not particularly unusual. CG-14 is quite low in vanadium. Although this can be a sign of condensation or evaporation under oxidizing conditions (DAVIS *et al.*, 1982), other elements which become volatile under oxidizing conditions, such as cerium and the refractory siderophiles, are not depleted relative to other refractory elements. Normal coarse-grained inclusions have vanadium enrichments ranging from 2.7 to 22.0 times C1 chondrites (CONARD, 1976; unpublished data from this labora-

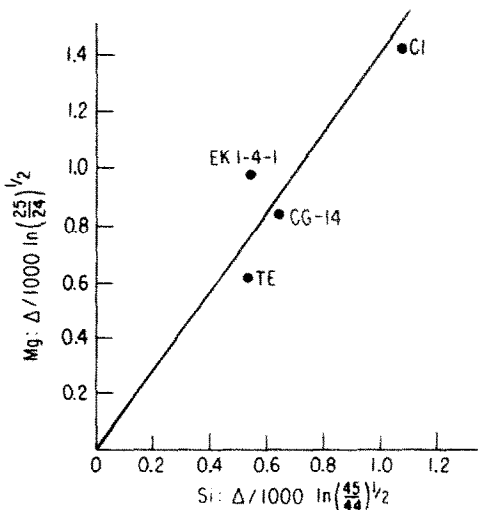


FIG. 11. Correlation between magnesium and silicon isotope fractionation. The measured fractionations have been normalized to the value of the inverse square-root of the masses, using Mg atoms for magnesium and SiO molecules for silicon.

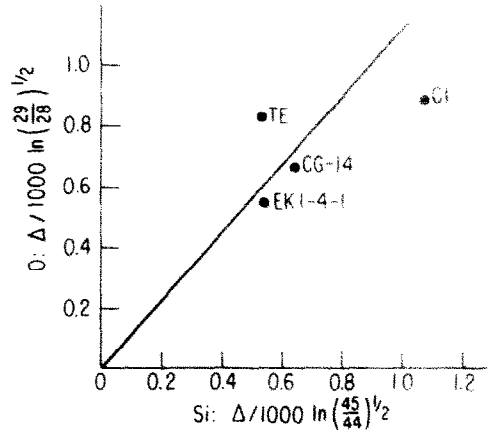


FIG. 12. Correlation between oxygen and silicon isotope fractionation, normalized as in Fig. 11, using CO molecules for oxygen and SiO molecules for silicon. The correlation of oxygen with silicon and magnesium is very weak.

tory). Compared with C1 and HAL, CG-14 is chemically rather unremarkable. A search for FUN inclusions based on unusual trace element patterns would have missed CG-14.

Isotopic constraints on the origin of CG-14 and TE

The magnitudes of the isotopic fractionations in the FUN inclusions are much too large to be attributable to condensation processes from "normal" nebular matter. They approach the values for kinetic fractionation of gaseous atoms or small molecules, *i.e.*, the inverse square root of the masses. These are: for Mg atoms, 20.4‰/mass unit; for Si atoms, 17.5‰/mass unit; for silicon in SiO molecules, 11.2‰/mass unit; and for oxygen in CO molecules, 17.5‰/mass unit. A rough correlation between magnesium and silicon fractionation effects can be seen in Fig. 11, in which the magnitude of each fractionation has been normalized to the inverse square root of the masses of Mg atoms and SiO molecules. The correlation is considerably poorer with the oxygen fractionations (Fig. 12). In particular, the oxygen fractionations in TE and C1 are almost identical, whereas the magnesium and silicon fractionations differ by about a factor of two. Such decoupling of magnesium and silicon from oxygen may not be too surprising, since magnesium and silicon are of similar volatility in the solar nebula, whereas oxygen forms a wide variety of compounds both more and less volatile than magnesium and silicon.

Isotopic fractionation by evaporative loss of magnesium and silicon might be sufficient to cause the variation of about 4‰/mass unit in silicon in "normal" Allende inclusions (MOLINI-VELSKO *et al.*, 1983), but would require prohibitively large loss to account for the much greater fractionations found in FUN inclusions. This is especially so for the olivine-rich inclusions, TE and CG-14, which have higher magnesium and silicon contents than most of the "ordinary" in-

clusions. It remains as one of the most remarkable characteristics of the FUN inclusions that they have undergone large isotopic fractionation of major elements without large chemical fractionation in comparison with other CAI in Allende.

A known astronomical site on which similarly large heavy-isotope enrichments of oxygen and silicon are produced is the surface of the moon (EPSTEIN and TAYLOR, 1971). In fact, if the isotopic data for FUN inclusions are plotted on the graph of $\delta^{30}\text{Si}$ versus $\delta^{18}\text{O}$ (Fig. 4 of Epstein and Taylor), it is found that the lunar and meteoritic data are well intermingled. The lunar effects have been attributed to removal of surficial material by micrometeorite vaporization and sputtering, fractionation in the lunar gravitational field and redeposition on grain surfaces (EPSTEIN and TAYLOR, 1971; CLAYTON *et al.*, 1974; KERRIDGE and KAPLAN, 1978; HOUSLEY, 1979). A major difference between the lunar and meteoritic observations is that the isotopic enrichment in the lunar samples occurs only for a very small fraction of the soil sample, which may be identifiable with the few-hundred Ångstrom-thick amorphous coatings observed by BIBRING *et al.* (1972). In FUN inclusions, on the other hand, it is the entire gram-sized inclusion that is isotopically enriched. Thus if an analogous set of processes led to the observed fractionations, then the vaporized or sputtered objects must have had dimensions not greater than some hundreds of Ångstroms, as has been concluded by D. CLAYTON (1981). Sputtering alone as a fractionation mechanism may be insufficient if the model of HAFF *et al.* (1981) is applicable. Their calculations indicate that sputtering of oxygen from silicates would produce fractionations considerably smaller than are seen in FUN inclusions, and in the opposite direction.

A further difficulty with the proposal that sputtering in interstellar space produces the FUN inclusions is that the non-FUN inclusions, which constitute about 95% of all Allende inclusions, must *each* re-accrete just the same amount of sputtered magnesium and silicon that they had lost (D. CLAYTON, 1981).

The model of WOOD (1981) for producing FUN and non-FUN inclusions is based on different rates of evaporative loss of magnesium, silicon and oxygen. This model is not very attractive in that inclusions with very distinctive textures, such as CG-14 and TE, are found in both the FUN and non-FUN categories. Experiments aimed at reproducing textures of Allende inclusions in the laboratory have shown that the textures depend very sensitively on the thermal history (PAQUE and STOLPER, 1983).

CONCLUSIONS

We have described two forsterite-, fassaite-, spinel-rich inclusions in Allende which, together with three previously described, share common mineralogy and texture. On the basis of their petrologic characteristics, we conclude that they were at least partially molten at temperatures greater than 1400°C, that the crys-

tallization sequence was spinel, olivine, fassaite and, finally, Mg-rich melilite and that at least some of them experienced partial volatilization of MgO and SiO₂ from their outer margins. At least one of these inclusions, CG-14, is highly enriched in MgO relative to CaO and Al₂O₃ compared to Allende coarse-grained inclusions, although it is just as strongly enriched in refractory trace elements as the latter, relative to C1 chondrites. Two of these objects, CG-14 and TE, are FUN inclusions on the basis of their oxygen, magnesium and silicon isotopic compositions. Thus, just as in the case of Ca-, Al-rich coarse-grained inclusions, some members of this forsterite-rich group have FUN isotopic properties and some do not. Volatilization of magnesium and silicon is not responsible for their isotopic fractionation, as this process would require prohibitively large mass loss from these magnesium-rich inclusions. Work by HAFF *et al.* (1981) suggests that sputtering from silicates may not be able to account for the magnitude and direction of oxygen isotope fractionation in FUN inclusions. FUN and non-FUN inclusions of each mineralogical type have remarkably similar textures, implying that FUN and non-FUN inclusions have similar thermal histories and arguing against their having suffered different rates of evaporative loss of major elements.

Acknowledgments—This work was supported by funds from the National Aeronautics and Space Administration through grants NGL 14-001-169 (RNC), NGR 14-001-249 (LG) and NAG 9-54 (LG) and from the National Science Foundation through grants EAR 78-23680 (RNC) and EAR 82-18154 (LG).

REFERENCES

- ALLEN J. M., GROSSMAN L., LEE T. and WASSERBURG G. J. (1980) Mineralogy and petrography of HAL, an isotopically-unusual Allende inclusion. *Geochim. Cosmochim. Acta* **44**, 685-699.
- BANNER A. E. and STIMPSON B. P. (1975) A combined ion probe/spark source analysis system. *Vacuum* **24**, 511-517.
- BLANDER M. and FUCHS L. H. (1975) Calcium-aluminum-rich inclusions in the Allende meteorite: evidence for a liquid origin. *Geochim. Cosmochim. Acta* **39**, 1605-1619.
- BIBRING J. P., DURAUD J. P., DURRIEU L., JOURET C., MAURETTE M. and MEUNIER R. (1972) Ultrathin amorphous coatings on lunar dust grains. *Science* **175**, 753-755.
- CLAYTON D. D. (1981) Some key issues in isotopic anomalies: Astrophysical history and aggregation. *Proc. Lunar Planet. Sci. Conf. 12th* **12B**, 1781-1802.
- CLAYTON R. N. and MAYEDA T. K. (1977) Correlated oxygen and magnesium isotope anomalies in Allende inclusions. I: Oxygen. *Geophys. Res. Lett.* **4**, 295-298.
- CLAYTON R. N. and MAYEDA T. K. (1983) Oxygen isotopes in eucrites, shergottites, nakhlites and chassignites. *Earth Planet. Sci. Lett.* **62**, 1-6.
- CLAYTON R. N., MAYEDA T. K. and HURD J. M. (1974) Loss of oxygen, silicon, sulfur, and potassium from the lunar regolith. *Proc. Lunar Sci. Conf. 5th*, 1801-1809.
- CLAYTON R. N., ONUMA N., GROSSMAN L. and MAYEDA T. K. (1977) Distribution of the pre-solar component in Allende and other carbonaceous chondrites. *Earth Planet. Sci. Lett.* **34**, 209-224.
- CONARD R. (1976) A study of the chemical composition of Ca-Al-rich inclusions from the Allende meteorite. M.S. thesis, Oregon State University.

- DAVIS A. M., GROSSMAN L. and ALLEN J. M. (1978) Major and trace element chemistry of separated fragments from a hibonite-bearing Allende inclusion. *Proc. Lunar Planet. Sci. Conf. 9th*, 1235-1247.
- DAVIS A. M., TANAKA T., GROSSMAN L., LEE T. and WASSERBURG G. J. (1982) Chemical composition of HAL, an isotopically-unusual Allende inclusion. *Geochim. Cosmochim. Acta* **46**, 1627-1651.
- DOMINIK B., JESSBERGER E. K., STAUDACHER TH., NAGEL K. and EL GORESY A. (1978) A new type of white inclusion in Allende: Petrography, mineral chemistry, ^{40}Ar - ^{39}Ar ages, and genetic implications. *Proc. Lunar Planet. Sci. Conf. 9th*, 1249-1266.
- EPSTEIN S. and TAYLOR H. P. JR. (1971) $\text{O}^{18}/\text{O}^{16}$, $\text{Si}^{30}/\text{Si}^{28}$, D/H , and $\text{C}^{13}/\text{C}^{12}$ ratios in lunar samples. *Proc. Lunar Sci. Conf. 2nd*, 1421-1441.
- ESAT T. M., PAPANASTASSIOU D. A. and WASSERBURG G. J. (1979) Trials and tribulations of ^{26}Al : Evidence for disturbed systems (abstract). In *Lunar and Planetary Science X*, pp. 361-363. Lunar and Planetary Inst., Houston.
- ESAT T. M., PAPANASTASSIOU D. A. and WASSERBURG G. J. (1980) The initial state of ^{26}Al and $^{26}\text{Mg}/^{24}\text{Mg}$ in the early solar system (abstract). In *Lunar and Planetary Science XI*, pp. 262-264. Lunar and Planetary Inst., Houston.
- GEE K. H. and OSBORN E. F. (1969) Phase equilibria at liquidus temperatures in a part of the system $\text{CaO-MgO-Al}_2\text{O}_3\text{-SiO}_2$: The system $\text{Ca}_2\text{MgSi}_2\text{O}_7\text{-Ca}_2\text{Al}_2\text{SiO}_7\text{-CaMgSi}_2\text{O}_6\text{-CaAl}_2\text{Si}_2\text{O}_8$. *Bull. Earth Min. Sci. Exper. Station Penn. State Univ. No. 85*, 23-51.
- GREY C. M., PAPANASTASSIOU D. A. and WASSERBURG G. J. (1973) The identification of early condensates from the solar nebula. *Icarus* **20**, 213-239.
- GROSSMAN L. (1975) Petrography and mineral chemistry of Ca-rich inclusions in the Allende meteorite. *Geochim. Cosmochim. Acta* **39**, 433-454.
- GROSSMAN L., GANAPATHY R. and DAVIS A. M. (1977) Trace elements in the Allende meteorite—III. Coarse-grained inclusions revisited. *Geochim. Cosmochim. Acta* **41**, 1647-1664.
- HAFF P. K., WATSON C. C. and TOMBRELLO T. A. (1981) Possible isotopic fractionation effects in material sputtered from minerals. *J. Geophys. Res.* **86**, 9553-9561.
- HOUSLEY R. M. (1979) A model for chemical and isotopic fractionation in the lunar regolith by impact vaporization. *Proc. Lunar Planet. Sci. Conf. 10th*, 1673-1683.
- HUNEKE J. C., ARMSTRONG J. T. and WASSERBURG G. J. (1983) FUN with PANURGE: High mass resolution ion microprobe measurements of Mg in Allende inclusions. *Geochim. Cosmochim. Acta* **47**, 1635-1650.
- HUTCHEON I. D. (1982) Ion probe magnesium isotope measurements of Allende inclusions. In *Nuclear and Chemical Dating Techniques: Interpreting the Environmental Record A.C.S. Symposium Series No. 176*, pp. 95-128.
- KERRIDGE J. F. and KAPLAN I. R. (1978) Sputtering: Its relationship to isotopic fractionation on the lunar surface. *Proc. Lunar Planet. Sci. Conf. 9th*, 1687-1709.
- LEE T. (1979) New isotopic clues to solar system formation. *Rev. Geophys. Space Phys.* **17**, 1591-1611.
- LEE T., RUSSELL W. A. and WASSERBURG G. J. (1979) Calcium isotopic anomalies and the lack of aluminum-26 in an unusual Allende inclusion. *Astrophys. J.* **228**, L93-L98.
- LEE T., MAYEDA T. K. and CLAYTON R. N. (1980) Oxygen isotopic anomalies in Allende inclusion HAL. *Geophys. Res. Lett.* **7**, 493-496.
- MACPHERSON G. J. and GROSSMAN L. (1981) Clastic rims on inclusions: Clues to the accretion of the Allende parent body (abstract). In *Lunar and Planetary Science XII*, pp. 646-647. Lunar and Planetary Inst., Houston.
- MACPHERSON G. J., GROSSMAN L., ALLEN J. M. and BECKETT J. R. (1981) Origin of rims on coarse-grained inclusions in the Allende meteorite. *Proc. Lunar Planet. Sci. Conf. 12th* **12B**, 1079-1091.
- MACPHERSON G. J., PAQUE J. M., STOLPER E. and GROSSMAN L. (1983) Reverse zoning in melilite and crystallization sequences in Allende Type B Ca-, Al-rich inclusions (abstract). In *Lunar and Planetary Science XIV*, pp. 456-457. Lunar and Planetary Inst., Houston.
- MOLINI-VELSKO C. (1983) Isotopic composition of silicon in meteorites. Ph.D. thesis. University of Chicago.
- MOLINI-VELSKO C., MAYEDA T. K. and CLAYTON R. N. (1983) Silicon isotopes in components of the Allende meteorite (abstract). In *Lunar and Planetary Science XIV*, pp. 509-510. Lunar and Planetary Inst., Houston.
- NAGASAWA H., BLANCHARD D. P., SHIMIZU H. and MASUDA A. (1982) Trace element concentrations in the isotopically unique Allende inclusion, EK 1-4-1. *Geochim. Cosmochim. Acta* **46**, 1669-1673.
- PAQUE J. M. and STOLPER E. (1983) Experimental evidence for slow cooling of Type B CAIs from a partially molten state (abstract). In *Lunar and Planetary Science XIV*, pp. 596-597. Lunar and Planetary Inst., Houston.
- STEELE I. M., HUTCHEON I. D., SOLBERG T. N., SMITH J. V. and CLAYTON R. N. (1977) Effect of energy selection on quantitative analysis in secondary ion microanalysis. *Int. J. Mass Spectrom. Ion Phys.* **23**, 293-305.
- STOLPER E. (1982) Crystallization sequences of Ca-Al-rich inclusions from Allende: An experimental study. *Geochim. Cosmochim. Acta* **46**, 2159-2180.
- WARK D. A. and LOVERING J. F. (1977) Marker events in the early evolution of the solar system: Evidence from rims on Ca-Al-rich inclusions in carbonaceous chondrites. *Proc. Lunar Sci. Conf. 8th*, 95-112.
- WARNER R. D. and LUTH W. C. (1973) Two-phase data for the join monticellite (CaMgSiO_4)-forsterite (Mg_2SiO_4): Experimental results and numerical analysis. *Amer. Mineral.* **58**, 998-1008.
- WASSERBURG G. J., LEE T. and PAPANASTASSIOU D. A. (1977) Correlated O and Mg isotope anomalies in Allende inclusions: II. Magnesium. *Geophys. Res. Lett.* **4**, 299-302.
- WOOD J. A. (1981) The interstellar dust as a precursor of Ca, Al-rich inclusions in carbonaceous chondrites. *Earth Planet. Sci. Lett.* **56**, 32-44.